ARTICLE

Fabrication of High-Quality In_2Se_3 Nanowire Arrays toward High-Performance Visible-Light Photodetectors

Tianyou Zhai,[†,‡,*] Xiaosheng Fang,[†,*] Meiyong Liao,[§] Xijin Xu,[†] Liang Li,[†] Baodan Liu,[†] Yasuo Koide,[§] Ying Ma,[‡,*] Jiannian Yao,[‡,*] Yoshio Bando,[†] and Dmitri Golberg[†]

[†]International Center for Materials Nanoarchitectonics (MANA), National Institute for Materials Science (NIMS), Namiki 1-1, Tsukuba, Ibaraki 305-0044, Japan, [‡]Beijing National Laboratory for Molecular Sciences (BNLMS), Institute of Chemistry, Chinese Academy of Sciences, Beijing, 100190, P. R. China, and [§]Sensor Materials Center, National Institute for Materials Science (NIMS), Namiki 1-1, Tsukuba, Ibaraki 305-0044, Japan

ABSTRACT The synthesis of high-quality In_2Se_3 nanowire arrays *via* thermal evaporation method and the photoconductive characteristics of In_2Se_3 individual nanowires are first investigated. The electrical characterization of a single In_2Se_3 nanowire verifies an intrinsic n-type semiconductor behavior. These single-crystalline In_2Se_3 nanowires are then assembled in visible-light sensors which demonstrate a fast, reversible, and stable response. The high photosensitivity and quick photoresponse are attributed to the superior single-crystal quality and large surface-to-volume ratio resulting in fewer recombination barriers in nanostructures. These excellent performances clearly demonstrate the possibility of using In_2Se_3 nanowires in next-generation sensors and detectors for commercial, military, and space applications.

KEYWORDS: indium selenide · nanowire arrays · photodetector · semiconductor · visible light · thermal evaporation · sensor

Nanowires are important building blocks for nanoscale optoelectronics, as they can be functioned as miniaturized devices and electrical interconnects.[1−11] Nanodevices, such as field-effect transistors, gas and chemical sensors, Schottky diodes, and memories have been reported.[12] These devices have demonstrated significant progress in the "bottom-up" approach for building new-generation electronic and photoelectronic systems.[13] As important devices, nanophotodetectors are essential elements in high-resolution imaging techniques and light-wave communications, as well as in future memory storage and optoelectronic circuits.[14−16] Various semiconductor materials, including group IV elements (Si, Ge), group III−V compounds (GaN, GaAs, InP), and group II−VI compounds (ZnS, ZnO, CdS, CdSe) have been used in photodetectors; however, most of them require a relatively long response time/decay time. This has limited the practical applications.

Indium selenide (In_2Se_3), an interesting compound semiconductor of the $A_2^{III}B_3^{VI}$ family with a layered structure, usually crystallizes into double layers of nonmetal atoms, each consisting of the [Se−In−Se−In−Se] sheets stacked together through the Se atoms along the *c*-axis,[17] as shown in Figure 1, inset. The strong intralayer bonding and the weak interlayer van der Waals interactions give rise to highly anisotropic structural, electrical, optical, and mechanical properties,[18] which make the In_2Se_3 phase attractive for photovoltaic solar cells, ionic batteries, optoelectronics and phase change memory devices.[19−27] Furthermore, In_2Se_3 is one of the most promising materials for detecting visible radiation due to its direct and narrow band gap, high absorption coefficient in the visible range, and high sensitivity.[28,29] However, the relatively low response speed (from several seconds to tens of minutes)[30−32] of In_2Se_3 films seriously restricts their applications in high-frequency or high-speed devices. Single-crystalline In_2Se_3 nanowires can be expected to have superior properties owing to their anisotropic photon geometry and large surface-to-volume ratio combined with the carrier and photon confinement in two dimensions. However, since the synthesis of high-quality, high-yield In_2Se_3 nanostructures is still a challenge, the reports on In_2Se_3 semiconductor nanowire-based nanodevices have been limited.[33,34] In this paper, we report on the fabrication of high-quality single-crystalline In_2Se_3 nanowire arrays and demonstrate the performance of a

*Address correspondence to zhai.tianyou@gmail.com, zhai.tianyou@nims.go.jp, fang.xiaosheng@nims.go.jp, yingma@iccas.ac.cn, jnyao@iccas.ac.cn.

Received for review September 18, 2009 and accepted February 3, 2010.

Published online February 10, 2010. 10.1021/nn9012466

single In_2Se_3 nanowire in a photoconductive device. Both of these topics, to the best of our knowledge, have never been discussed before. The results imply that the In_2Se_3 nanowires are prospective candidates for applications in high-sensitivity and high-speed nanoscale photodetectors and photoelectronic switches.

RESULTS AND DISCUSSION

The representative morphologies and structures of the produced In_2Se_3 nanostructures were investigated by field-emission scanning electron microscopy (FESEM), as shown in Figure 1 and Supporting Information, Figure S1. The SEM images show that the ordered arrays of In_2Se_3 nanowires uniformly and compactly cover the substrates. The nanowires have smooth surfaces and possess a uniform diameter of 50−100 nm, and a typical length of several tens of micrometers. A transmission electron microscope (TEM) image of a single In_2Se_3 nanowire is displayed in Figure 2a, which demonstrates that the nanowire has uniform diameter throughout the length. Statistics based on numerous TEM images (more than 100 nanostructures were analyzed) indicates that the diameters of the nanowires are *ca.* 50−100 nm. An X-ray energy-dispersive spectrum (EDS) acquired from an individual nanowire exhibits strong In and Se peaks, and the atomic ratio of In and Se is close to the 2:3 stoichiometry, as expected. The Cu peak in the inset of Figure 2a is due to the TEM grid. Line-scanning elemental profile across the In_2Se_3 nanowire (white line in Figure 2a) is shown in Figure 2b. The profiles of In and Se both show a broad peak in the structure center that directly reveals the nanowire morphology. The elemental maps displayed in Figures 2c,d shed the light on the distribution of each constituting element and further verify the entire uniformity of their distribution throughout the structure. The perfect crystallinity of the nanowire was further confirmed by high-resolution (HR) TEM and selected-area electron diffraction (SAED). Figure 2e is a HRTEM image of the nanowire, which clearly shows the hexagonal lattice planes with the spacings of 0.35 and 0.96 nm, in accord with the (100) and (002) planes of the hexagonal α-In_2Se_3 (JSPDS-00-034-1279), respectively. The axis of the nanowire is parallel to the [100] direction, indicating that the nanowires have been grown along this direction. The superb crystal quality and largely reduced number of grain boundaries and/or other interfaces (which usually act as recombination sites in polycrystalline materials) should lead to improved electron transport properties.[35,36] What should be mentioned is that no In_2Se_3 nanowire growth was observed on the same substrates when the Au catalysts were not in use (Supporting Information, Figure S2). It is thus obvious that Au played an important role in the growth of In_2Se_3 nanowire arrays. The Au nanoparticles serve as ideal nucleation sites for the preferential absorption of vaporized reactants, such as In and Se vapors and In_2Se_3 molecules due to their large accommodation coefficient.[37,38] Thus the Au−In−Se eutectic alloy droplets are formed owing to their lower eutectic point of 575 °C.[33] These then lead to the nucleation and growth of In_2Se_3 nanowires through the VLS process when the alloy droplets become saturated with respect to In_2Se_3.[39,40] The absence of Au particles at the nanowire tips may be due to the exfoliation of Au particles during the growth process.

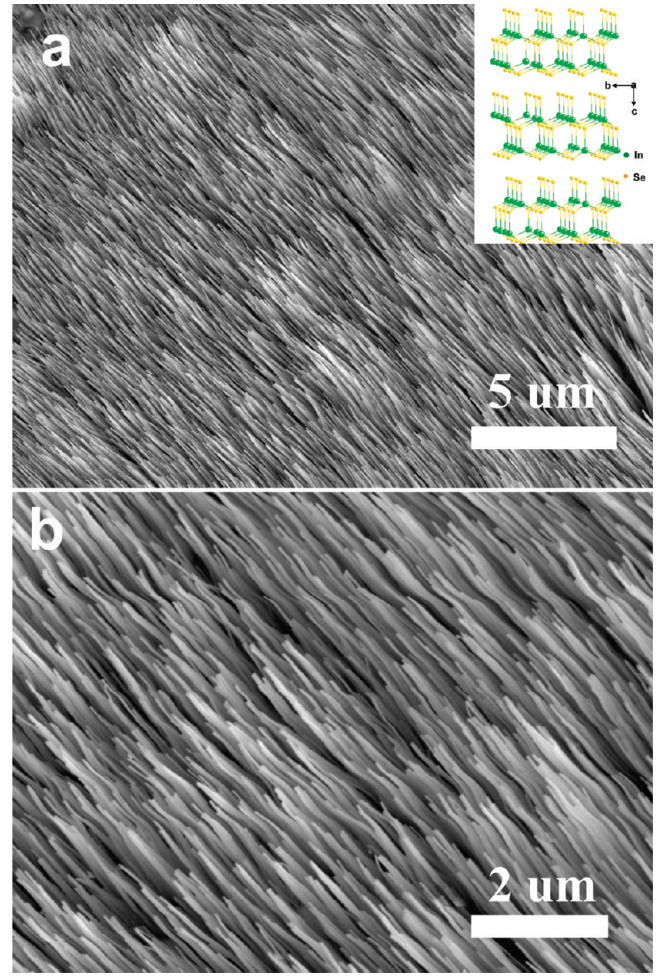

Figure 1. SEM images of as-synthesized In_2Se_3 nanowire arrays. Inset: structure model of In_2Se_3 layered structure.

An individual In_2Se_3 nanowire was configured as the field-effect transistor device on a p-type degenerately doped Si substrate covered with a 200 nm thick SiO_2 layer, which is schematically shown in the inset of Figure 3. The current−voltage ($I_{sd}-V_{sd}$) characteristics of an In_2Se_3 nanowire FET device at different gate voltages (from +20 to −20 V with a 10 V step) are shown in Figure 3. The current *versus* source-drain voltage and gate voltage were measured. It can be clearly seen that the conductance of the NW decreases as the gate potential decreases, demonstrating that the In_2Se_3 NW is an n-type semiconductor, in accord with bulk In_2Se_3.[17,41] This n-type behavior is mainly attributed to the Se vacancies generated during the synthesis process.

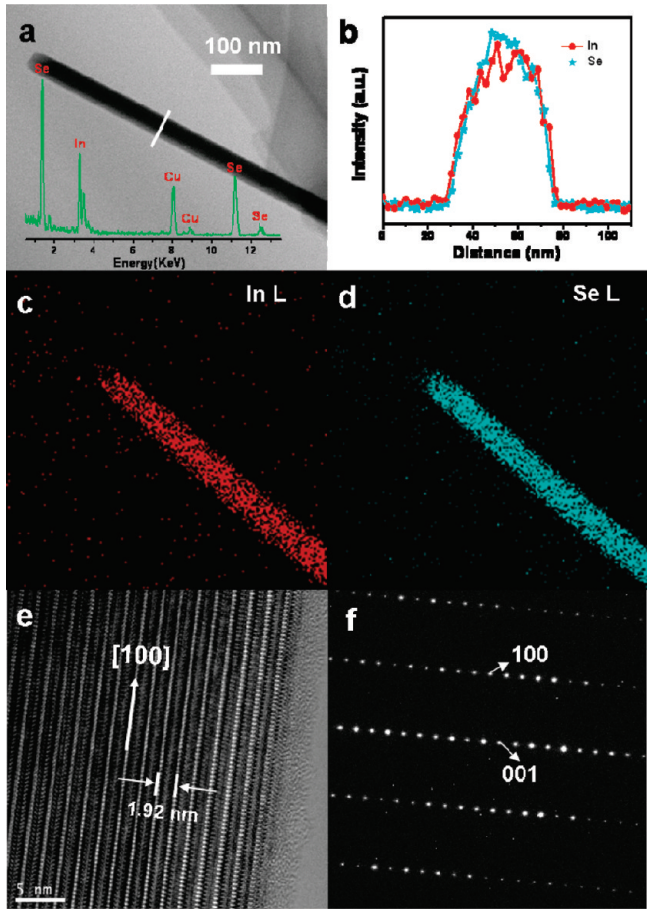

Figure 2. (a) TEM image and the corresponding EDS spectrum (inset) of an individual In_2Se_3 nanowire; (b) line-scan (indicated by a white line in a) profile displaying In and Se spatial distribution across the In_2Se_3 nanowire; (c, d) spatially resolved EDS elemental maps depicting the distribution of the constituting elements within the nanowire; the images correspond to the In L-edge and Se L-edge signals, respectively; (e, f) HRTEM image and the corresponding SAED pattern of the nanowire verifying that it grew along [100] direction.

Photogenerated carriers could significantly increase the conductivity when a semiconductor material is illuminated by photons with the energy higher than the bandgap.[42,43] In this work, for the first time, the photoconductivity of In_2Se_3 nanowire was investigated. The SEM image of the In_2Se_3 single-nanowire device photoresponse is shown in the upper inset in Figure 4b. The 10 nm/100 nm Ti/Au parallel electrodes were deposited on the nanowire dispersed on a SiO_2/Si substrate, and the uncovered part of the nanowire was exposed to the incident light. The diameter of this nanowire and the channel length were 80 nm and 1 μm, respectively. Figure 4a is a schematic diagram of the device configuration for the photocurrent measurements under light illumination. The $I-V$ measurements were performed by using a two-probe method. Figure 4b shows typical $I-V$ curves of a single In_2Se_3 nanowire, measured in the dark conditions and under 500 nm-light illumination (2.81 mW/cm^2), respectively. The approximately linear shape of the curves indicates good Ohmic contacts established between the nanowire and the electrodes. Furthermore, under visible light illumination the current across the nanowire dramatically increases compared to the dark current. Figure 4c shows the time response of the In_2Se_3 nanowire device to the pulsed incident 500 nm-light created by a manual chopper. The "on"- and "off"-state currents for each of five cycles shown here remain the same within the noise level, indicating the reversibility and stability of In_2Se_3 optical switches over this time interval. The possible origins of the observed current fluctuations are surface species absorption/desorption or appearance of defects.[44] The photocurrent values reveal that no pumping or priming effects should be taken into account for the explored time scale. A closer examination of time responses (Figure 4d) shows that they consist of flat photocurrent plateaus and are characterized by short rising and dark decay times; both being 0.3 s (the limit of the present experimental setup). Thus, we may suggest that the real photoconductivity response time is even faster than ~0.3 s. Compared with other nanostructure-based optical sensors made of ZnO,[45,46] GaN,[47,48] CdS,[49] SnO_2,[50] RuO_2/TiO_2,[51] *etc.*, the present In_2Se_3 nanowire sensors show a faster time response and persistent photoconductivity. For example, a CdS nanobelt-based white-light photoconductor possesses the rise time of 1 s and the decay time of 3 s,[49] a ZnO nanowire-based UV sensor (by utilizing Schottky contacts and surface functionalization) has the rise time of 0.6 s and the decay time of 0.8 s,[46] and a RuO_2/TiO_2 core/shell nanowire-based UV photodetector exhibits the rise time of 307 s and the decay time of 437 s.[51] Several unique characteristics of the present In_2Se_3 nanowire device are thought to significantly improve the observed responsivity compared to previous devices: (1) The superior crystal quality (the density of traps induced by defects is thus dramatically reduced and the photocurrent rapidly reaches a steady state both on rise and decay stages).[13] (2) The larger surface-to-volume ratio (the dangling bonds on the nanowire surface can

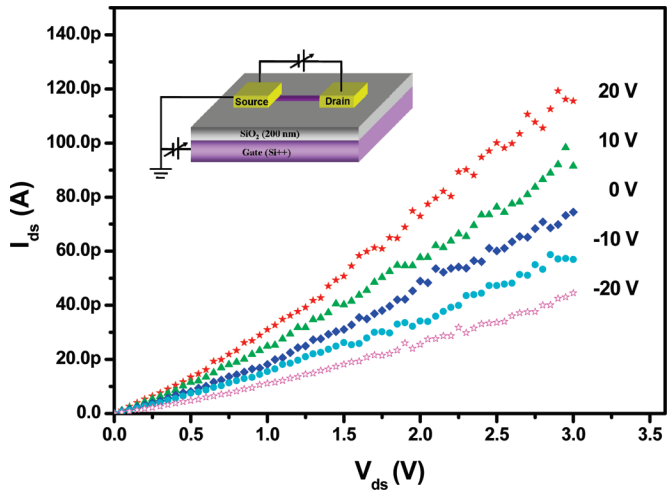

Figure 3. Gate-dependent $I-V$ characteristics of a single In_2Se_3 nanowire at room temperature. Inset: schematic view of the In_2Se_3 nanowire-based FET configuration.

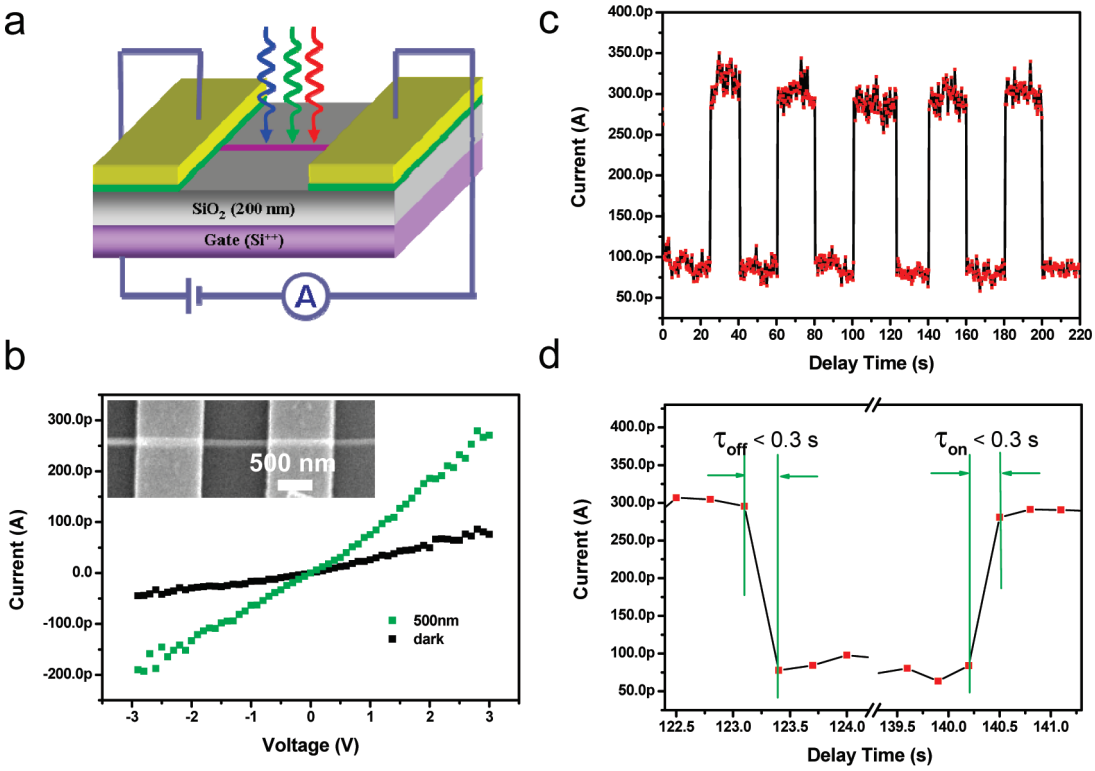

Figure 4. (a) A schematic diagram of the device configuration for the photocurrent measurements; (b) *I*−*V* curves of the single In_2Se_3 nanowire in the dark conditions and under 500 nm-light illumination, 2.81 mW/cm^2, respectively. The inset shows a SEM image of the single-nanowire device. (c) Time dependent photocurrent response of the In_2Se_3 nanowire device to 500 nm pulsed incident light with a period of ~20 s at an applied voltage of 3 V. (d) The enlarged portions of 122.4−124.2 s and 139.3−141.2 s ranges (from light-off to light-on states) showing ultimately fast time response (beyond the limit of our measurement setup of 0.3 s).

serve as recombination centers for photogenerated carriers, which would enhance the free carriers' recombination and shorten the decay time). (3) The shorter channel (a short channel can result in shortening the photocarrier transit time, thus increasing the responsivity).[52,53] (4) The lower recombination barrier (band bending usually occurs at the semiconductor surface due to Fermi-level pinning, which results in a recombination barrier for electron−hole pairs). The latter is consistent with the previous observations of GaN nanowires,[54] CdS nanoribbons,[13] and methyl-squarylium nanowires.[35]

The detector current responsivity (R_λ), defined as the photocurrent generated per unit power of the incident light on the effective area of a photoconductor,[55] and the external quantum efficiency (EQE), defined as the number of electrons detected per incident photon, are critical parameters for photoconductors. The large values of R_λ and EQE correspond to high sensitivity. The R_λ and EQE can be calculated as $R_\lambda = I_\lambda/(P_\lambda S)$[56,57] and EQE $= hcR_\lambda/(e\lambda)$.[58,59] Here, I_λ is the photocurrent, P_λ is the light intensity, S is the effective illuminated area, h is the Planck's constant, c is the velocity of light, e is the electronic charge, and λ is the exciting wavelength. According to our experimental results, the R_λ and EQE of a In_2Se_3 single-nanowire device are ~89 A/W and ~22000%, respectively, for the incident wavelength of 500 nm at 3 V. These numbers are much higher compared to other semiconductor detectors.[13] All these results imply that the In_2Se_3 nanowires are promising candidates for applications in high-selectivity, high-sensitivity, and high-speed nanoscale photodetectors and photoelectronic switches.

Interestingly, the number of nanowires within a device significantly affects the current and response speed, as shown in Figure 5. The photocurrent of a two-nanowire device declines quickly from 290 pA (under light illumination) to a dark current of 155 pA, while that of a multi-nanowire device drops relatively slowly from 2100 to 1200 pA. Compared with the results for the single-nanowire and two-nanowire devices, the multinanowire device has a higher dark current, and a photocurrent, lower ratios of photocurrent/dark current, and a slower decay time. The higher dark current for the multinanowire device is due to the smaller nanowire resistance and the lower contact resistance caused by the larger contact area of the multinanowire to the electrodes, while the higher photocurrent is simply due to the larger exposed area. Furthermore, the decay curve of the multi-nanowire devices consists of two fitted straight lines with different slopes. Thus two different time constants, t_1 (<0.3 s) for the fast decay, and t_2 (14 s) for the slow de-

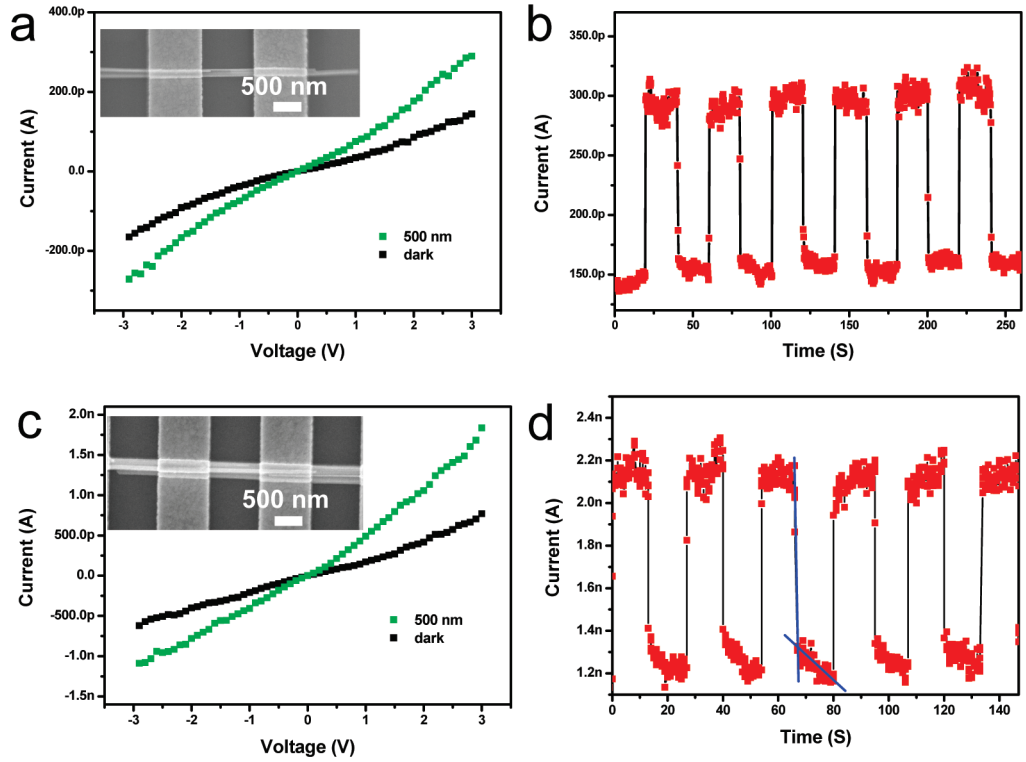

Figure 5. (a, c) SEM images and typical *I*−*V* characteristics of devices fabricated with two nanowires and several nanowires, respectively, on the electrode; (b, d) corresponding time response of a photocurrent upon 500 nm light illumination measured for light-on and -off states.

cay tail, are distinguished in the decay curve. The appearance of a slow decay tail in the multinanowire detector is likely due to the carrier trapping at the interfaces between the nanowires. Since the fast decay dominates the overall response, the slow component in the photocurrent does not degrade the photoresponse properties.

CONCLUSIONS

For the first time we present the synthesis of high-quality In_2Se_3 nanowire arrays *via* thermal evaporation method and demonstrate the photoconductive characteristics of an individual In_2Se_3 nanowire. The synthesized In_2Se_3 nanowires are single-crystals grown along the [100] direction with a uniform diameter of 50−100 nm and a typical length of tens of micrometers. A single In_2Se_3 nanowire shows an intrinsic n-type semiconductor behavior. Being assembled in visible-light sensors, the nanowires exhibit a fast, reversible, and stable response. The high photosensitivity and quick photoresponse are attributed to the perfect single-crystal quality, large surface-to-volume ratio, and fewer recombination barriers within the nanostructures. The documented excellent performances open up the unique possibilities of using In_2Se_3 nanowires for the next-generation photosensors and photodetectors in commercial, military, and space applications.

METHODS

Synthesis and characterization of In_2Se_3 nanowires. The synthesis of In_2Se_3 nanowires was conducted in a horizontal tube furnace with a 50 mm inner-diameter quartz tube placed inside. In short, commercial In_2Se_3 and graphite powders with a weight ratio of 1:2 were mixed, ground, and then loaded on an alumina boat and positioned at the center of the tube. Several single-crystal Si wafers, cleaned by a standard procedure and covered with Au nanoparticles, were placed downstream to act as deposition substrates. Prior to heating, the furnace tube was purged with high-purity Ar for 3 h in order to eliminate any oxygen in the furnace. The flow rate and pressure inside the tube were kept, respectively, at 60 SCCM and 130 Pa throughout the experiments. The system was rapidly heated to 900 °C in 60 min and kept at this temperature for 240 min. Then it was cooled down to room temperature. The synthesized products were characterized by a scanning electron microscope (SEM, Hitachi F-4300) and a transmission electron microscope (HRTEM, JEM-3000F) equipped with an X-ray energy dispersive spectrometer (EDS).

Preparation of Single In_2Se_3 Nanowire Device. To fabricate single-nanowire detectors, the In_2Se_3 nanowires were removed by sonication from the substrate and subsequently dispersed in ethanol. The solution was dropped on a thermally oxidized Si substrate covered with a 200 nm SiO_2 layer. Two electrodes together with their bonding pads were exposed by electron-beam lithography. After the development, a Ti/Au (10 nm/ 100 nm) film was deposited over the structure followed by a lift-off process.

Measurements of a Nanowire Device. The current−voltage (*I*−*V*) characteristics of an individual In_2Se_3 nanodevice were measured using an Advantest picoammeter R8340A and a dc voltage source R6144. Gate voltages were applied to the p^+-Si substrate in standard global back-gate geometry. The time responses of sensors to light illumination were measured by a current meter after shutting the light.

Acknowledgment. T. Y. Zhai thanks the Japan Society for the Promotion of Science (JSPS) for a support in the form of a fellowship tenable at the National Institute for Materials Science (NIMS), Tsukuba, Japan. This work was supported by the World Premier International Research Center (WPI) initiative on Materials Nanoarchitectonics (MANA), MEXT, Japan. This work was also in part supported by the National Natural Science Foundation of China (No. 20733006, 50720145202), and the National Basic Research Program of China (No. 2006CB806200, 2007CB936402). The authors are indebted to Mr. S. G. Ri, Mr. Y. Misawa, Mr. H. Sugaya, and Mr. K. Ohno for their technical assistances and kind help.

Supporting Information Available: SEM images of In_2Se_3 nanowire arrays, and SEM image of the synthesized In_2Se_3 products without using Au catalysts. This material is available free of charge *via* the Internet at http://pubs.acs.org.

REFERENCES AND NOTES

1. Rao, C. N. R.; Müller, A.; Cheetham, A. K. *Nanomaterials Chemistry: Recent Developments and New Directions*; John Wiley: Hoboken, NJ, 2007.
2. Kind, H.; Yan, H. Q.; Messer, B.; Law, M.; Yang, P. D. Nanowire Ultraviolet Photodetectors and Optical Switches. *Adv. Mater.* **2002**, *14*, 158.
3. Shen, G. Z.; Chen, P. C.; Ryu, K.; Zhou, C. W. Devices and Chemical Sensing Applications of Metal Oxide Nanowires. *J. Mater. Chem.* **2009**, *19*, 828.
4. Fang, X. S.; Bando, Y.; Liao, M. Y.; Zhai, T. Y.; Gautam, U. K.; Li, L.; Koide, Y.; Golberg, D. An Efficient Way to Assemble ZnS Nanobelts as Ultraviolet-Light Sensors with Enhanced Photocurrent and Stability. *Adv. Funct. Mater.* **2010**, *20*, 500.
5. Zhai, T. Y.; Fang, X. S.; Bando, Y.; Dierre, B.; Liu, B. D.; Zeng, H. B.; Huang, Y.; Xu, X. J.; Yuan, X. L.; Sekiguchi, T.; Golberg, D. Characterization, Cathodoluminescence, and Field-Emission Properties of Morphology-Tunable CdS Micro/Nanostructures. *Adv. Funct. Mater.* **2009**, *19*, 2423.
6. Fang, X. S.; Xiong, S. L.; Zhai, T. Y.; Bando, Y.; Liao, M. Y.; Gautam, U. K.; Koide, Y.; Zhang, X. G.; Qian, Y. T.; Golberg, D. High-Performance Bule/Ultraviolet-Light-Sensitive ZnSe-Nanobelt Photodetectors. *Adv. Mater.* **2009**, *21*, 5016.
7. Pan, Z. W.; Dai, Z. R.; Wang, Z. L. Nanobelts of Semiconducting Oxides. *Science* **2001**, *291*, 1947.
8. Zhai, T. Y.; Zhong, H. Z.; Gu, Z. J.; Peng, A. D.; Fu, H. B.; Ma, Y.; Li, Y. F.; Yao, J. N. Manipulation of the Morphology of ZnSe Submicron Structures Using CdSe Nanocrystals as the Seeds. *J. Phys. Chem. C* **2007**, *111*, 2980.
9. Ye, C. H.; Fang, X. S.; Hao, Y. F.; Teng, X. M.; Zhang, L. D. Zinc Oxide Nanostructures: Morphology Derivation and Evolution. *J. Phys. Chem. B* **2005**, *109*, 19758.
10. Ye, C. H.; Meng, G. W.; Wang, Y. H.; Jiang, Z.; Zhang, L. D. On the Growth of CdS Nanowires by the Evaporation of CdS Nanopowders. *J. Phys. Chem. B* **2002**, *106*, 10338.
11. Zhai, T. Y.; Fang, X. S.; Bando, Y.; Liao, Q.; Xu, X. J.; Zeng, H. B.; Ma, Y.; Yao, J. N. Morphology-Dependent Stimulated Emission and Field Emission of Ordered CdS Nanostructure Arrays. *ACS Nano* **2009**, *3*, 949.
12. Lin, D. D.; Wu, H.; Pan, W. Photoswitches and Memories Assembled by Electrospinning Aluminum-Doped Zinc Oxide Single Nanowires. *Adv. Mater.* **2007**, *19*, 3968.
13. Jie, J. S.; Zhang, W. J.; Jiang, Y.; Meng, X. M.; Li, Y. Q.; Lee, S. T. Photoconductive Characteristics of Single-Crystal CdS Nanoribbons. *Nano Lett.* **2006**, *6*, 1887.
14. Jiang, Y.; Zhang, W. J.; Jie, J. S.; Meng, X. M.; Fan, X.; Lee, S. T. Photoresponse Properties of CdSe Single-Nanoribbon Photodetectors. *Adv. Funct. Mater.* **2007**, *17*, 1795.
15. Liao, M. Y.; Koide, Y.; Alvarez, J.; Imura, M.; Kleider, J. P. Persistent Positive and Transient Absolute Negative Phtoconductivity Observed in Diamond Photodetectors. *Phys. Rev. B* **2008**, *78*, 045112.
16. Zhai, T. Y.; Fang, X. S.; Liao, M. Y.; Xu, X. J.; Zeng, H. B.; Bando, Y.; Golberg, D. A Comprehensive Review of One-Dimensional Metal-Oxide Nanostructure Photodetectors. *Sensors* **2009**, *9*, 6504.
17. Julien, C.; Hatzikraniotis, E.; Kambas, K. Electrical Transport-Properties of Impurity-Doped In_2Se_3. *Phys. Stat. Sol. A* **1986**, *97*, 579.
18. Shen, G. Z.; Chen, D.; Chen, P. C.; Zhou, C. W. Vapor-Solid Growth of One-Dimensional Layer-Structured Gallium Sulfide Nanostructures. *ACS Nano* **2009**, *3*, 1115.
19. Lakshmikumar, S. T.; Rastogi, A. C. Selenization of Cu and In Thin Films for the Preparation of Selenide Photoabsorber Layers in Solar Cells Using Se Vapour Source. *Sol. Energy Mater. Sol. Cells* **1994**, *32*, 7.
20. Lyu, D. Y.; Lin, T. Y.; Lin, J. H.; Tseng, S. C.; Hwang, J. S.; Chiang, H. P.; Chiang, C. C.; Lan, S. M. Growth and Properties of Single-Phase γ-In_2Se_3 Thin Films on (111) Si Substrate by AP-MOCVD using H_2Se Precursor. *Sol. Energy Mater. Sol. Cells* **2007**, *91*, 888.
21. Julien, C.; Hatzikraniotis, E.; Chevy, A.; Kambas, K. Electrical Behavior of Lithium Intercalated Layer In−Se Compounds. *Mater. Res. Bull.* **1985**, *20*, 287.
22. Ye, J. P.; Soeda, S.; Nakamura, Y.; Nittono, O. Crystal Structures and Phase Transformation in In_2Se_3 Compound Semiconductor. *Jpn. J. Appl. Phys.* **1998**, *37*, 4264.
23. Peng, H. L.; Schoen, D. T.; Meister, S.; Zheng, X. F.; Cui, Y. Synthesis and Phase Transformation of In_2Se_3 and $CuInSe_2$ Nanowires. *J. Am. Chem. Soc.* **2007**, *129*, 34.
24. Vaidyanathan, R.; Stickney, J. L.; Cox, S. M.; Compton, S. P.; Happek, U. Formation of In_2Se_3 Thin Films and Nanostructures Using Electrochemical Atomic Layer Epitaxy. *J. Electroanal. Chem.* **2003**, *559*, 55.
25. Lai, K. J.; Peng, H. L.; Kundhikanjana, W; Schoen, D. T.; Xie, C.; Meister, S.; Cui, Y.; Kelly, M. A.; Shen, Z. X. Nanoscale Electronic Inhomogeneity in In_2Se_3 Nanoribbons Revealed by Microwave Impedance Microscopy. *Nano Lett.* **2009**, *9*, 1265.
26. Peng, H. L.; Xie, C.; Schoen, D. T.; Cui, Y. Large Anisotropy of Electrical Properties in Layer-Structured In_2Se_3 Nanowires. *Nano Lett.* **2008**, *8*, 1511.
27. Yu, B.; Ju, S.; Sun, X. H.; Ng, G.; Nguyen, T. D.; Meyyappan, M.; Janes, D. B. Indium Selenide Nanowire Phase-Charge Memory. *Appl. Phys. Lett.* **2007**, *91*, 133119.
28. Sánchez-Royo, J. F.; Segura, A.; Lang, O.; Schaar, E.; Pettenkofer, C.; Jaegermann, W.; Roa, L.; Chevy, A. Optical and Photovoltaic Properties of Indium Selenide Thin Films Prepared by van der Waals Epitaxy. *J. Appl. Phys.* **2001**, *90*, 2818.
29. Bouzouita, H.; Bouguila, N.; Duchemin, S.; Fiechter, S.; Dhouib, A. Preparation and Characterization of In_2Se_3 Thin Films. *Renewable Energy* **2002**, *25*, 131.
30. Watanabe, I.; Sekiya, T. Extremely Long-Lived Residual Photocurrent in Amorphous In_2Se_3 Films. *Jpn. J. Appl. Phys.* **1989**, *28*, 638.
31. Sreekumar, R.; Jayakrishnan, R.; Kartha, C. S.; Vijayakumar, K. P. Anomalous Photoconductivity in γ In_2Se_3. *J. Appl. Phys.* **2006**, *100*, 033707.
32. Sreekumar, R.; Jayakrishnan, R.; Kartha, C. S.; Vijayakumar, K. P.; Khan, S. A.; Avasthi, D. K. Enhancement of Band Gap and Photoconductivity in Gamma Indium Selenide Due to Swift Heavy Ion Irradiation. *J. Appl. Phys.* **2008**, *103*, 023709.
33. Sun, X. H.; Yu, B.; Ng, G.; Nguyen, T. D.; Meyyappan, M. III−VI Compound Semiconductor Indium Selenide (In_2Se_3) Nanowires: Synthesis and Application. *Appl. Phys. Lett.* **2006**, *89*, 233121.
34. Peng, H. L.; Zhang, X. S.; Twesten, R. D.; Cui, Y. Vacancy Ordering and Lithium Insertion in III_2VI_3 Nanowires. *Nano Res.* **2009**, *2*, 327.
35. Zhang, X. J.; Jie, J. S.; Zhang, W. F.; Zhang, C. Y.; Luo, L. B.; He, Z. B.; Zhang, X. H.; Zhang, W. J.; Lee, C. S.; Lee, S. T. Photoconductivity of a Single Small-Molecule Organic Nanowire. *Adv. Mater.* **2008**, *20*, 2427.
36. Merritt, V. Y. Organic Photovoltaic Materials: Squarylium and Cyanine-TCNQ Dyes. *IBM J. Res. Dev.* **1978**, *22*, 353.
37. Barrelet, C. J.; Wu, Y.; Bell, D. C.; Lieber, C. M. Synthesis of CdS and ZnS Nanowires Using Single-Source Molecular Precursors. *J. Am. Chem. Soc.* **2003**, *125*, 11498.

38. Gao, T.; Wang, T. H. Catalytic Growth of In_2O_3 Nanobelts by Vapor Transport. *J. Cryst. Growth* **2006**, *290*, 660–664.
39. Li, C.; Zhang, D. H.; Han, S.; Liu, X. L.; Tang, T.; Zhou, C. W. Diameter-Controlled Growth of Single-Crystalline In_2O_3 Nanowires and Their Electronic Properties. *Adv. Mater.* **2003**, *15*, 143.
40. Morales, A. M.; Lieber, C. M. A Laser Ablation Method for the Synthesis of Crystalline Semiconductor Nanowires. *Science* **1998**, *279*, 208.
41. Fotsing, J.; Julien, C.; Balkanski, M. Annealing and Doping Effects in Layered In_2Se_3 Compounds. *Mater. Sci. Eng., B* **1998**, *1*, 139.
42. Liao, L.; Yan, B.; Hao, Y. F.; Xing, G. Z.; Liu, J. P.; Zhao, B. C.; Shen, Z. X.; Wu, T.; Wang, L.; Thong, J. T. L.; *et al*. P-Type Electrical, Photoconductive, and Anomalous Ferromagnetic Properties of Cu_2O Nanowires. *Appl. Phys. Lett.* **2009**, *94*, 113106.
43. Prades, J. D.; Jimenez-Diaz, R.; Hernandez-Ramirez, F.; Fermandez-Romero, L.; Andreu, T.; Cirera, A.; Romano-Rodriguez, A.; Cornet, A.; Morante, J. R.; Barth, S.; *et al*. Toward a Systematic Understanding of Photodetectors Based on Individual Metal Oxide Nanowires. *J. Phys. Chem. C* **2008**, *112*, 14639.
44. Fang, X. S.; Bando, Y.; Liao, M. Y.; Gautam, U. K.; Zhi, C. Y.; Dierre, B.; Liu, B. D.; Zhai, T. Y.; Sekiguchi, T.; Koide, Y.; Golberg, D. Single-Crystalline ZnS Nanobelts as Ultraviolet-Light Sensors. *Adv. Mater.* **2009**, *21*, 2034.
45. Li, Y. B.; Valle, F. D.; Simonnet, M.; Yamada, I.; Delaunay, J. J. High-Performance UV Detector Made of Ultra-Long ZnO Bridging Nanowires. *Nanotechnology* **2009**, *20*, 045501.
46. Zhou, J.; Gu, Y. D.; Lu, Y. F.; Mai, W. J.; Yeh, P. H.; Bao, G.; Sood, A. K.; Polla, D. L.; Wang, Z. L. Gigantic Enhancement in Response and Reset Time of ZnO UV Nanosensor by Utilizing Schottky Contact and Surface Functionalization. *Appl. Phys. Lett.* **2009**, *94*, 191103.
47. Wu, H.; Sun, Y.; Lin, D. D.; Zhang, R.; Zhang, C.; Pan, W. GaN Nanofibers Based on Electrospinning: Facile Synthesis, Controlled Assembly, Precise Doping, and Application as High Performance UV Photodetector. *Adv. Mater.* **2009**, *21*, 227.
48. Han, S.; Jin, W.; Zhang, D. H.; Tang, T.; Li, C.; Liu, X. L.; Liu, Z. Q.; Lei, B.; Zhou, C. W. Photoconduction Studies on GaN Nanowire Transistors under UV and Polarized UV Illumination. *Chem. Phys. Lett.* **2004**, *389*, 176.
49. Gao, T.; Li, Q. H.; Wang, T. H. CdS Nanobelts as Photoconductors. *Appl. Phys. Lett.* **2005**, *86*, 173105.
50. Mathur, S.; Barth, S.; Shen, H.; Pyun, J. C.; Werner, U. Size-Dependent Photoconductance in SnO_2 Nanowires. *Small* **2005**, *1*, 713.
51. Chueh, Y. L.; Hsieh, C. H.; Chang, M. T.; Chou, L. J.; Lao, C. S.; Song, J. H.; Gan, J. Y.; Wang, Z. L. RuO_2 Nanowires and RuO_2/TiO_2 Core/Shell Nanowires: From Synthesis to Mechanical, Optical, Electrical, and Photoconductive Properties. *Adv. Mater.* **2007**, *19*, 143.
52. Chen, R. S.; Wang, S. W.; Lan, Z. H.; Tsai, J. T. H.; Wu, C. T.; Chen, L. C.; Chen, K. H.; Huang, Y. S.; Chen, C. C. On-Chip Fabrication of Well-Aligned and Contact-Barrier-Free GaN Nanobridge Devices with Ultrahigh Photocurrent Responsivity. *Small* **2008**, *4*, 925.
53. Kung, P.; Zhang, X.; Walker, D.; Saxler, A.; Piotrowski, J.; Rogalski, A.; Razeghi, M. Kinetics of Photoconductivity in n-Type GaN Photodetectors. *Appl. Phys. Lett.* **1995**, *67*, 3792.
54. Calarco, R.; Marso, M.; Richter, T.; Aykanat, A.; Meijers, R.; Hart, A. V. D.; Stoica, T.; Lüth, H. Size-Dependent Photoconductivity in MBE-Growth GaN-Nanowires. *Nano Lett.* **2005**, *5*, 981.
55. Morkoc, H.; Carlo, A. D.; Cingolani, P. GaN-Based Modulation Doped FETs and UV Detectors. *Solid-State Electron.* **2002**, *46*, 157.
56. Cheng, J. P.; Zhang, Y. J.; Guo, R. Y. ZnO Microtube Ultraviolet Detectors. *J. Cryst. Growth* **2008**, *310*, 57.
57. Ueda, T.; An, Z. H.; Hirakawa, K.; Komiyama, S. Charge-Sensitive Infrared Phototransistors: Characterization by an All-Cryogenic Spectrometer. *J. Appl. Phys.* **2008**, *103*, 093109.
58. Chen, X. P.; Zhu, H. L.; Cai, J. F.; Wu, Z. Y. High-Performance 4H-SiC-based Ultraviolet p-i-n Photodetector. *J. Appl. Phys.* **2007**, *102*, 024505.
59. Alamaviva, S.; Marinelli, M.; Milani, E.; Prestopino, G.; Tucciarone, A.; Verona, C.; Verona-Rinati, G.; Angelone, M.; Pillon, M. Extreme UV Photodetectors Based on CVD Single Crystal Diamond in a P-type/Intrinsic/Metal Configuration. *Diamond Relat. Mater.* **2009**, *18*, 101.